The role of magnetic equilibria in determining ECE in MAST

INSTITUTE OF PLASMA PHYSICS
ACADEMY OF SCIENCES OF THE CZECH REPUBLIC

UKAEA Fusion Working in Europe

J. Preinhaelter[1)], V. Shevchenko[2)], M. Valovič[2)], H. Wilson[2)], J. Urban[1)], P. Pavlo[1)], L. Vahala[3)], G. Vahala[4)]

[1)] EURATOM/IPP.CR Association, Institute of Plasma Physics, 182 21 Prague, Czech Republic

[2)] EURATOM/UKAEA Fusion Association, Culham Science Centre, Abingdon, OX14 3DB, UK

[3)] Old Dominion University, Norfolk, VA 23529, USA, [4)] College of William & Mary, Williamsburg, VA 23185, USA

Abstract

ECE simulation based on EFIT and SCENE magnetic equilibria in MAST is compared with detected signal. Nice fit is found for the L-modes and ELMy H-mode where both models give the same results. ECE from ELM-free H-mode has rather intricate structure and our models do not fit well with experiment. Simulation, based on EFIT, predict proper number of EC bands but their position is better estimated by SCENE which takes into account the edge currents.

ECE and EBW in MAST

- Extensive ECE data are available for MAST (Mega Ampere Spherical Tokamak) in the frequency range 16-60GHz
- The low magnetic field and high plasma density do not permit the usual radiation of O and X modes from the first five electron cyclotron harmonics
- Only electron Bernstein waves (EBW), which are unaffected by the density limits, can be responsible for the measured radiation
- The EBW are converted to the X mode in the upper hybrid resonance (UHR), which then propagates outside the plasma or it is converted to the O mode in the plasma resonance. The mode converted O mode then propagates outside the plasma

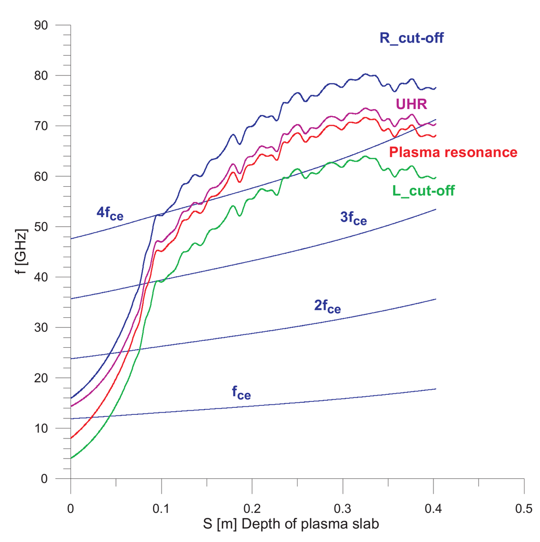

Fig. 1: Cutoffs and resonances in MAST cold plasma for normal incidence, shot #7798, 240ms

MAST ECE antenna system

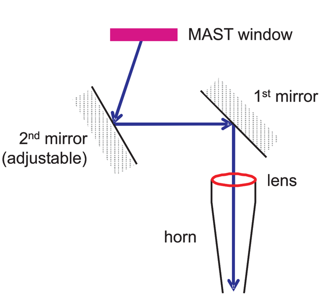

Fig. 2: MAST ECE antenna system setup

- The MAST ECE antenna system consists of a horn, two mirrors (the second one is adjustable) and the plasma-vacuum window (fig. 2)
- The wave propagation through the system is solved by Gaussian beam formalism
- At the 1st waist (w_{01}, see fig. 4) the beam is detached from the horn, the 2nd waist w_{02} is the projection of w_{01} by the lens

- Only linearly polarized waves are detected by the radiometer
- The polarization is changed at the mirrors

$$\vec{E}_{ref} = -\vec{E}_{inc} + 2\vec{N}_m\left(\vec{E}_{inc}\cdot\vec{N}_m\right)$$

- At the window the wave is partly reflected (see fig. 3) and its polarization becomes slightly elliptical

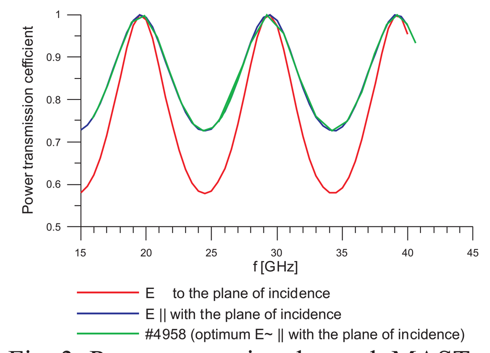

Fig. 3: Power transmitted trough MAST window (N_{quartz}=1.97, thickness=0.08m), incident ray j_{dev}=18°, j_{long}=22°, the angle of incidence on window = 28°

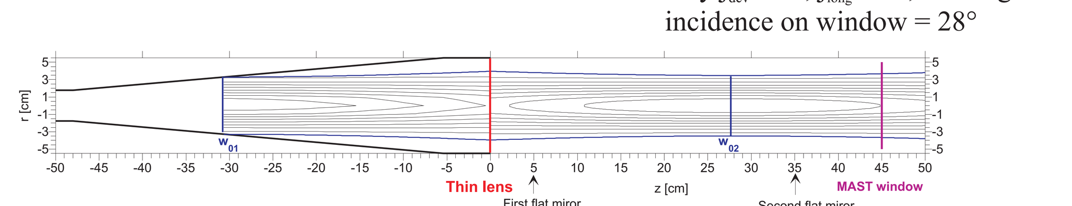

Fig. 4: Intensity of Gaussian beam in MAST antenna system for f=40GHz, $W_{01,02}$ are the waist positions

Simulated ECE power detected by the antenna

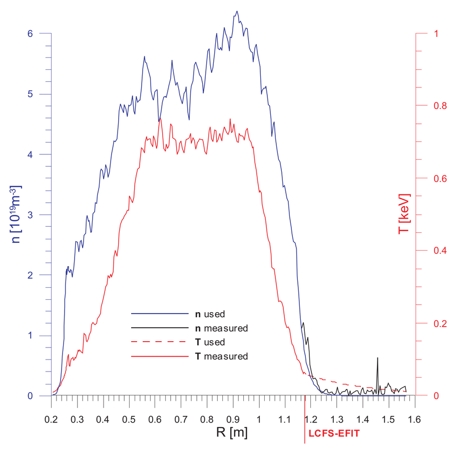

Fig. 5: Density and electron temperature profiles for the shot #7798

3D plasma model

- A realistic 3D model of the MAST plasma has been developed for the simulation. The magnetic field is reconstructed by splining of the two potentials determined by the EFIT code, assuming toroidal symmetry
- The temperature and density profile are obtained from the Thomson scattering measurements, beyond the LCFS exponentially decaying profiles are used
- Separate sets of straight rays are used to project the rim of window and the visible area to the second waist plane. Such an approach takes into account the shape of Gaussian beam in a near antenna and in far antenna regions properly
- Intersection of the antenna beam with the LCFS (last closed flux surface) determines the position of the spot used for the ray-tracing and conversion efficiency computations

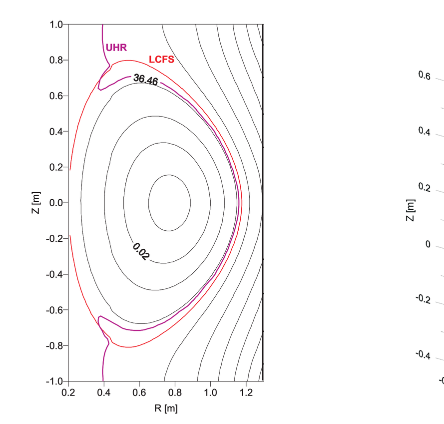

Fig. 6: magnetic potential for the shot #7798, time 240ms, UHR=36.46GHz

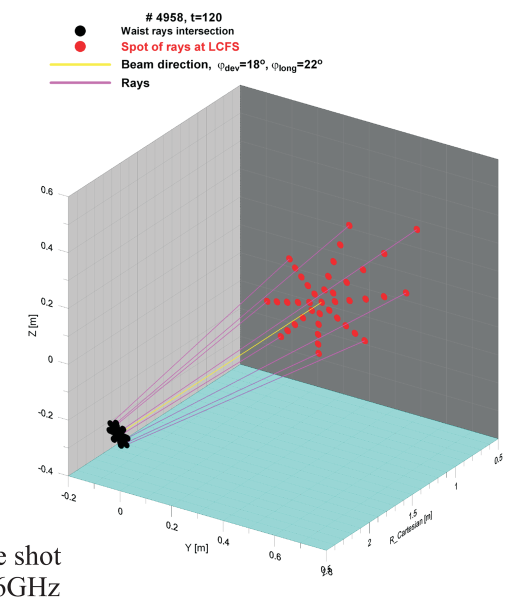

Fig. 7: Intersection of the antenna beam with the LCFS

Conversion efficiency computation

- Fullwave solution of the Maxwell's equations in the weakly collisional cold plasma slab is used for determination of the EBW-X-O conversion efficiency. This implies numerical solution of a set of the 2nd order ODE's with a singularity at UHR

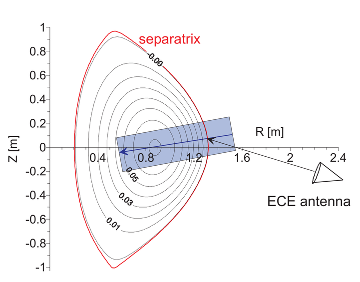

Fig. 8: Plasma slab construction

- At the intersection of the rays with the LCFS ("spots") we construct an auxiliary plane stratified slab inhomogeneous along the local density gradient
- The power absorbed in the vicinity of the upper hybrid resonance due to weak collisions corresponds (if n/fà0) exactly to the power converted to the electron Bernstein waves. The reverse process is adequate for ECE because we can assume reciprocity between emission and absorption
- The conversion efficiency must be computed for all (41 in our code) rays at each frequency in the frequency range. Recently developed code with adaptive mesh refinement is used for fast computation

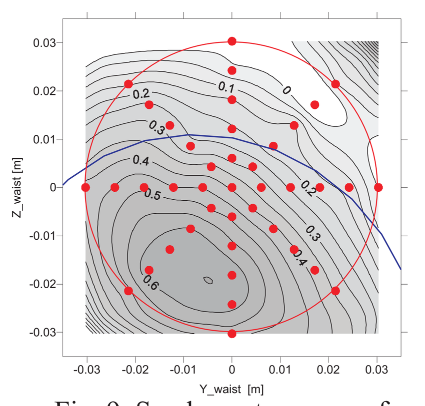

Fig. 9: Samle contour map of conversion efficiency projected to the second waist plane

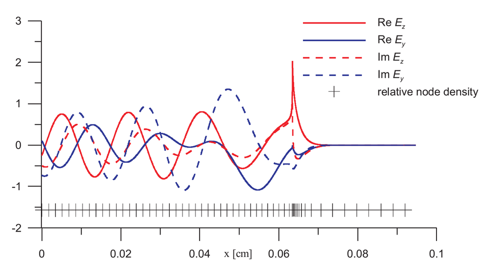

Fig. 10: Sample electric field computed by the adaptive finite

ECE intensity

- The intensity of ECE detected by the antenna can be expressed as

$$I_{ECE} = const \times \iint \mathrm{d}S\, W_{Gauss} C_{EBW-X-O}\,\omega^2 T_{rad} C_{window} V_{relat}$$

$W_{Gauss} = e^{-\left(2r^2/w_0^2\right)}$	Gauss weight (w_0 is the wais radius)
$C_{EBW-X-O}$	conversion efficiency
w^2T	Rayleigh-Jeans black body radiation law
C_{window}	power transmission coefficient of the MAST window
$V_{relat} = w^2/w_0^2$	relative visible area (w is the Gaussian beam radius at the plasma surface)

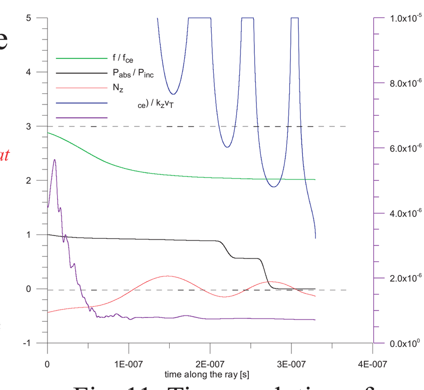

Fig. 11: Time evolution of 36.46GHz ray #1, shot #7798,

Radiative temperature and EBW absorption

- Ray-tracing code is used for the motion of EBW packet. The evolution equation for the power has to be integrated simultaneously with the ray dP/dt=-2g(t)P
- Non-local reabsorption of the radiation is described by the radiative transfer equation dP/dt=h-aP, which must be solved simultaneously with the ray evolution equation
- The emitted power can be expressed by Rayleigh-Jeans law with T_{rad} instead of local temperature T: P~w^2T_{rad}

$$T_{rad} = \int_0^\infty 2\gamma(t')\exp\left[-\int_0^{t'} 2\gamma(t'')\mathrm{d}t''\right]\mathrm{d}t'$$

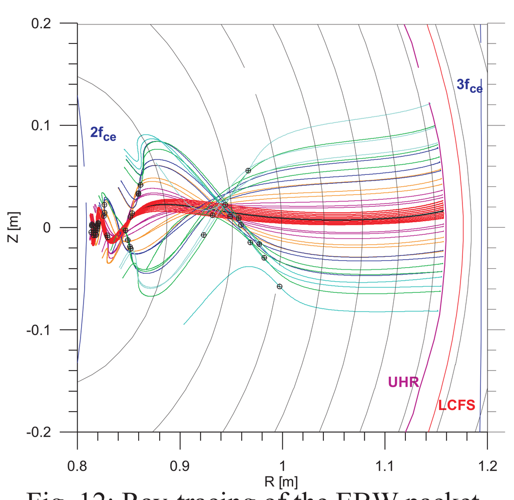

Fig. 12: Ray-tracing of the EBW packet, shot #7798, 240ms, f=36.46GHz

Beam direction and equilibria effects for #7798 L-mode and #4958 ELMy H-mode

Effects of the beam direction

- The best fit between measured and simulated ECE is obtained when different beam directions are assumed theoretically over the experimental antenna adjustment

Explanation:

- Beam direction is determined with precision to ±5°
- Diffraction of beam in rarefied plasma in SOL
- Magnetic equilibrium differs from that determined by EFIT

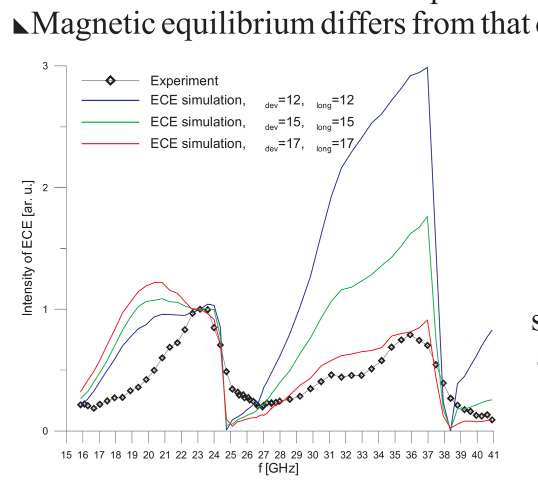

Fig. 13: ECE from MAST, shot #7798, time 240ms, reference frequency 23.14GHz. The fit is significantly improved with appropriate beam direction

Comparison of ECE simulation for EFIT and SCENE equilibria

#7798 L-mode

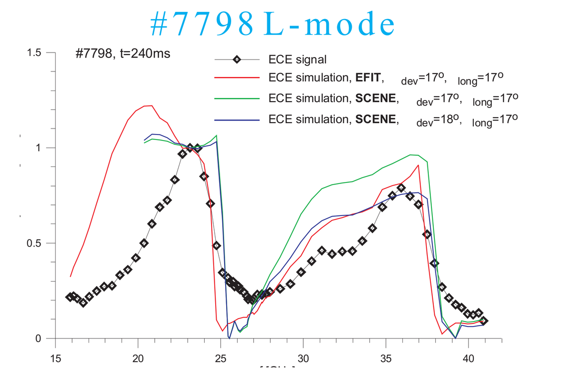

Fig. 14: Shot #7798 L-mode, ECE simulation fits well to detected signal for L-modes, SCENE [3] and EFIT gives similar results. Waves with f<23 GHz are converted in SOL where plasma density strongly fluctuates and our model of ECE does not catch this situation properly.

#4958 ELMy H-mode

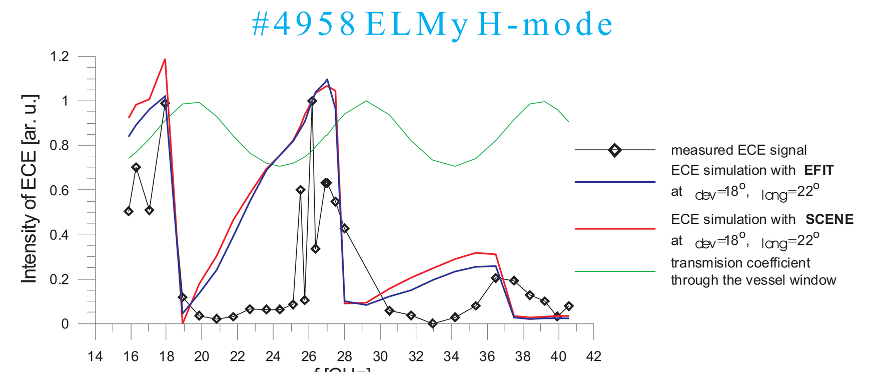

Fig. 15: With the appropriate beam angles the agreement with the experiment is good for both SCENE and EFIT equilibria but the decreases of ECE at the beginning of the second and the third EC band are not described well by any of the simulations. This is typical for ELMy H-modes.

ECE from #8694 ELM-free H-mode

Resonance topology

- Radial profiles of characteristic resonances at beam spot demonstrate clearly the difference in equilibria.

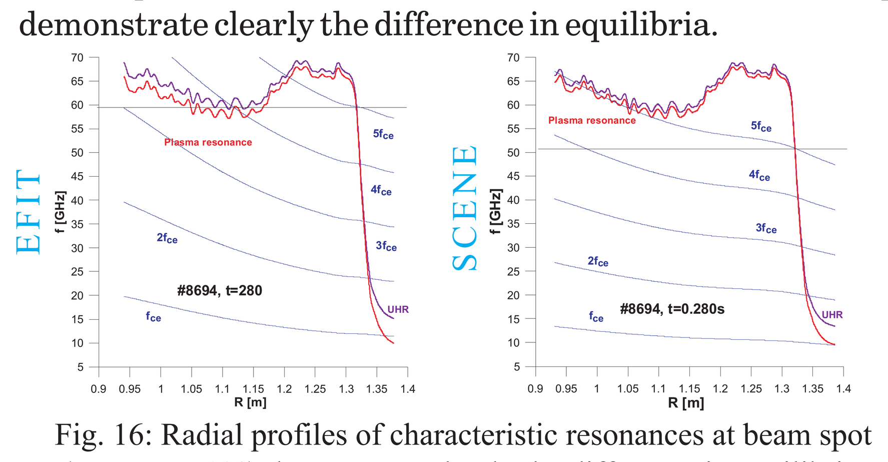

Fig. 16: Radial profiles of characteristic resonances at beam spot (dev= long=12°) demonstrate clearly the difference in equilibria.

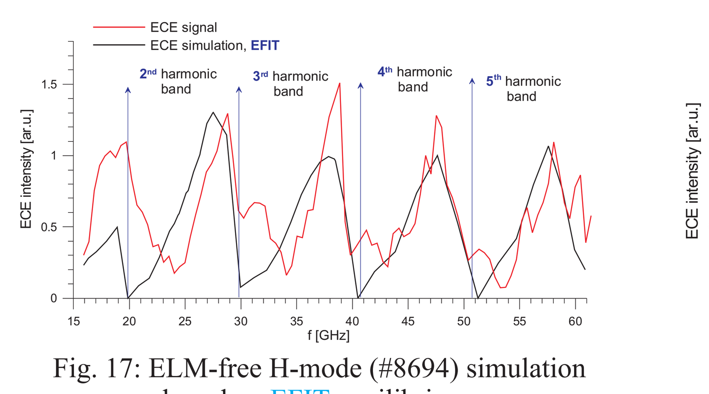

Fig. 17: ELM-free H-mode (#8694) simulation based on EFIT equilibrium.

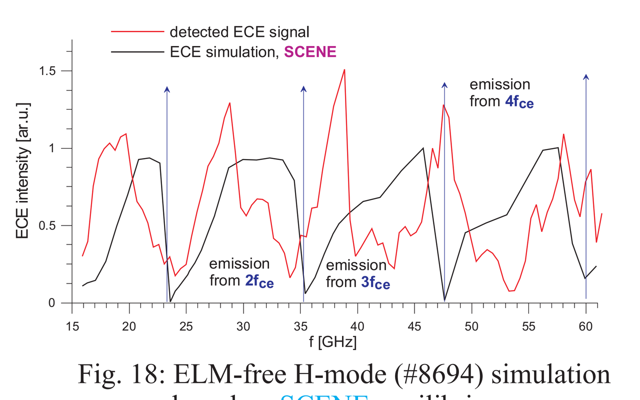

Fig. 18: ELM-free H-mode (#8694) simulation based on SCENE equilibrium.

EFIT

- Simulated and detected signal do not require additional beam aiming adjustment (new antenna calibration works well)
- Magnetic field at UHR predicted by EFIT is too low (periodicity of the detected ECE requires f_{ce}=11 GHz, but EFIT gives f_{ce}<10 GHz)
- Shapes of the peaks in the simulated EFIT signal in higher bands resemble well the detected signal

SCENE

- Surface currents considered in SCENE enhance magnetic field at UHR, but f_{ce}=12 GHz is too high
- Shapes of peaks of simulated signal do not correspond to the detected ones.
- Only four bands do not correspond to five band in detected signal

Ray-tracing can explain the peaks shapes in EFIT simulation

- Detailed evolution of central rays was studied for frequencies slightly below & slightly above the plasma surface electron cyclotron harmonics.

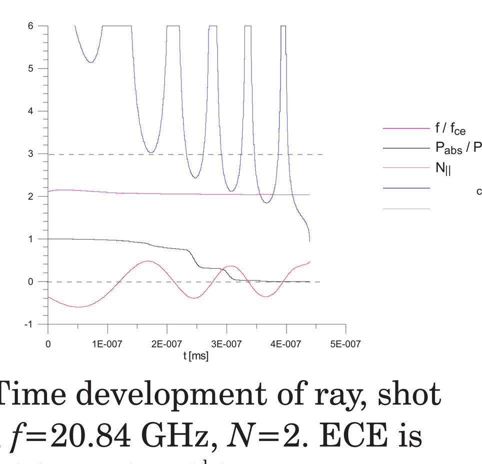

Fig. 19: Time development of ray, shot #8694, f=20.84 GHz, N=2. ECE is radiated from the 2nd harmonic. $N_{||}$ strongly oscillates and the absorption is highly non-local. The absorption in the 3rd harmonic is negligible.

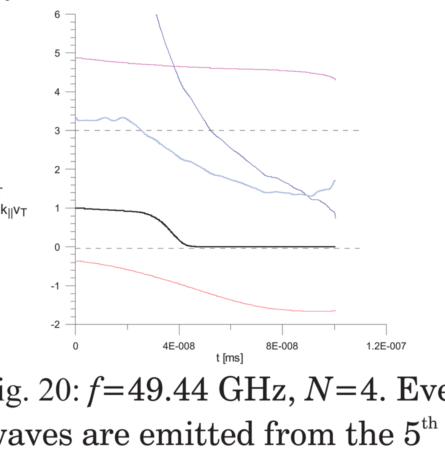

Fig. 20: f=49.44 GHz, N=4. Even if $f<5f_{ce}$, waves are emitted from the 5th harmonic. Because the factor $|(-5 _{ce})/N_{||}v_T|$ decreases faster then $|(-4 _{ce})/N_{||}v_T|$. $|N_{||}|$ increases monotonically and reaches 1 at the absorption region.

Space dependence of characteristic resonances in MAST

- Waves are emitted from well of the electron cyclotron resonances.
- #8694, t=0.280s, $_{dev}$=12°, $_{long}$=12°. We depicted situation at the end of EBW ray, when $|N_{||}|=1$ for waves having f slightly bellow Nf_{ce} at the plasma boundary and $|N_{||}|=0.36$ for waves having f slightly above Nf_{ce} at the plasma boundary. Broadening of Nf_{ce} is given by the factor $1/(1\pm 3N_{||}v_T/c)$

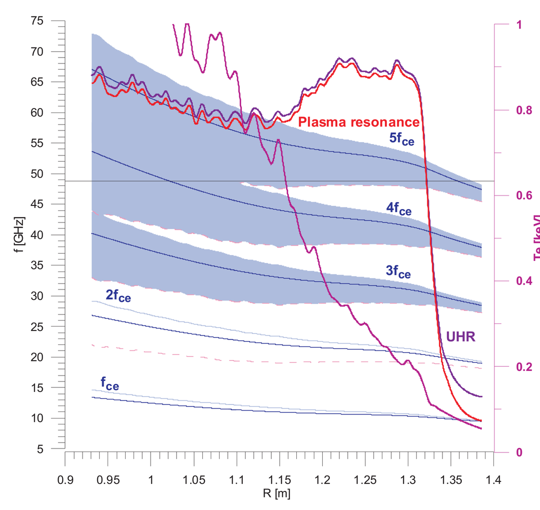

Conclusions

- Current theoretical model incorporates nearly all the details of the MAST.
- ECE antenna and plasma model based on experimental data.
- For L-mode, agreement between calculated and experimental EBW emission is good.
- For ELMy H-mode, agreement is good but model does not explain the smaller signal at lower frequency part within each harmonic bands.
- For ELM-free H-mode, simulation based on EFIT equilibrium agrees with experiment at higher harmonics while using SCENE equilibrium provides higher magnetic field at the plasma surface and better agreement at lower harmonics.
- These results show that EBW emission can provide an additional constraint for equilibrium reconstruction.

Acknowledgement

Part of this work was funded jointly by UK Engineering and Phys. Sci. Council and by EURATOM. We would like to appreciate valuable discussions with J. Zajac.

References

[1] Shevchenko V. et al., 15th RF Power in Plasma, Moran, 2003, edit. C. Forest, AIP 694, 359.
[2] Laqua H.P., et al., review, 15th RF Power in Plasma, Moran, 2003, edit. C. Forest, AIP 694, 15.
[3] H.R. Wilson: SCENE, UKAEA FUS 271 (1974), Culham, Abingdon, UK
[4] Preinhaelter J. e al, 15th RF Power in Plasma, Moran, 2003, edit. C. Forest, AIP 694, 388.
[5] Urban J.: Adaptive Finite Elements Method for the Solution of the Maxwell Equations in an Inhomogeneous Magnetized Plasma, Diploma thesis, Czech Technical University in Prague, 2004
[6] Preinhaelter J., Kopecky V., J. Plasma Phys. 10, 1 (1973), part 1.
[7] Pavlo P., Krlin L., Tluchor Z., Nucl. Fusion 31, 711 (1991).
[8] Goldsmith P.: Quasioptical systems: Gaussian Beam Quasioptical Propagation and Applications, Wiley-IEEE Press (1997)